Urban Climate 67 (2026) 102864

Contents lists available at ScienceDirect

Urban Climate

journal homepage: www.elsevier.com/locate/uclim

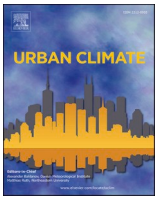

Estimating multi-scale ventilation corridors in complex 3D urban space: A graph-based least-cost path model

Yifan Luo [a], Xinyu Yu [a,**], Majid Nazeer [a], Man Sing Wong [a,b,c,d,e,*], Jinxin Yang [f], Rui Zhu [g,h]

[a] Department of Land Surveying and Geo-Informatics, The Hong Kong Polytechnic University, Hung Hom, Hong Kong, China
[b] Research Institute for Sustainable Urban Development, The Hong Kong Polytechnic University, Hung Hom, Hong Kong, China
[c] Research Institute of Land and Space, The Hong Kong Polytechnic University, Kowloon, Hong Kong, China
[d] State Key Laboratory of Climate Resilience for Coastal Cities, The Hong Kong Polytechnic University, Hong Kong, China
[e] Otto Poon Research Institute for Climate-Resilient Infrastructure, The Hong Kong Polytechnic University, Hong Kong, China
[f] School of Geography and Remote Sensing, Guangzhou University, Guangzhou, China
[g] State Key Laboratory of Climate System Prediction and Risk Management, Nanjing Normal University, Nanjing 210023, China
[h] Key Laboratory of Virtual Geographic Environment (Nanjing Normal University), Ministry of Education, Nanjing 210023, China

ARTICLE INFO

Keywords:
3D least-cost path model
Ventilation corridors
Urban microclimate
Least-cost path algorithm
Computational fluid dynamics

ABSTRACT

Cities are becoming denser and taller, posing increasing challenges for optimizing urban ventilation. Accurately identifying Ventilation Corridors (VCs) is therefore critical to alleviate the urban heat island effect, improve urban air quality, and enhance urban planning and design. However, traditional two-dimensional (2D) methods cannot accurately represent complex vertical airflow dynamics, resulting in the impacts of the depth dimension being ignored, especially in compact-high urban environments. To address this issue, we proposed a graph-based 3D Least-Cost Path (LCP) algorithm based on a voxel-based 3D urban model to identify both vertical and horizontal VCs in the complex urban area of Kowloon Peninsula in Hong Kong. Specifically, the optimal major VCs were determined using a shortest-path searching algorithm and validated by Computational Fluid Dynamics (CFD) simulations. Results show that the proposed model effectively identifies high-performance ventilation pathways, where wind speeds within the VCs are about 1.43 times the global wind speed at all resolutions and wind directions. Notably, the number of VCs per unit time decreases exponentially as the resolution becomes finer, with computational throughput dropping from 12,379 paths/s at 100 m resolution to 6246 paths/s at 50 m and 1351 paths/s at 30 m resolution. It indicates the robust scalability of our 3D LCP model to flexibly balance computational efficiency and spatial precision. Overall, the proposed 3D LCP model is promising to more accurately describe urban air flow, thereby supporting microclimate improvement and sustainable urban design in high-density cities.

* Corresponding author at: Department of Land Surveying and Geo-Informatics, The Hong Kong Polytechnic University, Hung Hom, Hong Kong, China.
** Corresponding author.
E-mail addresses: xin-yu.yu@connect.polyu.hk (X. Yu), Ls.charles@polyu.edu.hk (M.S. Wong).

https://doi.org/10.1016/j.uclim.2026.102864
Received 6 July 2025; Received in revised form 9 March 2026; Accepted 12 March 2026
Available online 23 March 2026

1. Introduction

Climate change and rapid urbanization have exacerbated weather extremes (Stott, 2016), as well as urban heat island (UHI) effect (Gartland, 2008). UHI intensity is defined as the temperature difference between urban and rural areas. It can be observed in a wide variety of cities of varying shapes and sizes and is one of the most distinctive features of urban climates (Luo et al., 2023; Stewart et al., 2014). Higher wind speeds can mitigate heat accumulation in the city to some extent, thus reducing UHI (Wong et al., 2010). In urban area, horizontal low-speed winds are usually associated with areas of high and complex surface roughness (Ng et al., 2011; Wicht et al., 2017). Therefore, optimizing wind flow in urban areas is critical to reducing heat accumulation, and ventilation corridors (VCs) have been recognized as an effective way to enhance air circulation in cities. Better urban ventilation system are effective in mitigating UHI and improving the urban microclimate.

Urban ventilation depends fundamentally on the ventilation corridors (VCs). VCs are characterized by low surface roughness and are aligned with the prevailing wind direction. But their precise dimensions and boundaries remain undefined (Ren et al., 2018). While VCs promote air circulation and heat mitigation, their efficacy is limited by urban morphology factors such as building density and vertical structure (Dang et al., 2022). Urban morphology can facilitate or impede wind flow, accelerating or decelerating the exchange of external fresh, cool air with urban air (Liu et al., 2025a, 2025b; Ma and Chen, 2022). In particular, building density has been shown to have a negative correlation with wind speed (Yuan and Ng, 2012), and neighborhood geometry also affects wind circulation (Zahid Iqbal and Chan, 2016). Therefore vertical structures and building density are critical factors for urban ventilation. Previous studies have used different methods to study VCs at specific scales and have been well validated in a robust manner. Currently, the common methods used to simulate VCs include: wind tunnel approach, Computational Fluid Dynamics (CFD) approach, and Geographic Information Science (GIS) technology (Bady et al., 2011; Montazeri et al., 2015; Yang and Li, 2015). Wind tunnel experiments are highly expensive and time consuming to build for large urban areas; CFD provides highly accurate results for complex airflow. However it requires massive computing power and extremely long simulation times. This slow process makes it unsuitable for testing multiple scenarios; GIS methods are efficient but usually lack the depth dimension. Most of these methods are limited to two-dimensional analyses or do not adequately reflect the depth and height components of urban morphology, which are critical to understanding the three-dimensional nature of airflow (Buccolieri and Hang, 2019; Fang and Zhao, 2022; Lu et al., 2022). Existing methods rely on simple 2D spatial assumptions. Tall buildings in high density areas force airflow to move vertically. Traditional 2D models cannot track these complex 3D paths. Therefore, they have significant limitations in resolving actual urban airflow processes. This limitation restricts the accurate assessment of vertical air exchange and weakens the scientific validity of ventilation potential identification. Only by introducing a systematic consideration of 3D spatial elements can effective VCs with the function of promoting vertical airflow be identified and evaluated. Thus, the development of an advanced 3D modeling framework is of great theoretical and practical significance for comprehensively portraying the urban airflow distribution and supporting the scientific optimization of ventilation strategies.

How can we reasonably develop a new 3D modeling framework? Among VCs spatial simulation methods, the least-cost path (LCP)

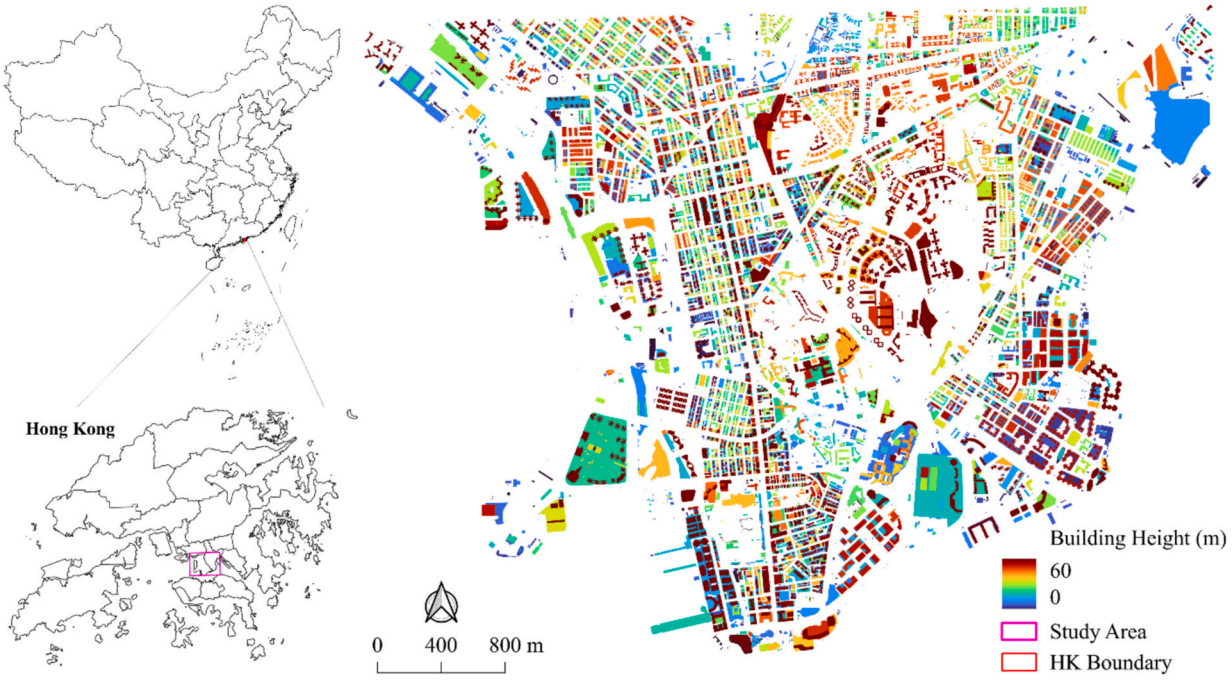

Fig. 1. Study area and building height distribution.

and the frontal area index (FAI) are widely used by researchers due to their computational efficiency and intuitive results (Luo et al., 2024; Qiao et al., 2017; Wong et al., 2011). These methods can indirectly reflect urban morphology in VCs studies through building heights, land use, and other characteristics. Most of these morphological parameters are under considered due to the limitations of existing approaches. A physical 3D urban space is needed for a comprehensive study of VCs (Wang et al., 2025). However, the urban space defined in previous studies usually ignores the depth dimension, or applying 3D space to VC analysis is challenging. Current methods focus only on VCs in 2D earth plane, VCs in 3D space are still not yet applicable.

This study pioneered the use of graph structures to construct a 3D urban space on which to base VC analysis. Our 3D LCP approach bridges the gap between spatial efficiency and vertical depth. It provides a much faster alternative to CFD, maintaining the 3D perspective which avoiding the extremely long simulation times. Based on the graph model constructed from the 3D space composition, we aim to apply graph-theoretic shortest path algorithms for identifying the VCs through the city. We will systematically analyze VCs in 3D urban space through three key steps. First, we will construct a 3D model of the Kowloon Peninsula, a typical high-density urban area, to accurately present the complex built environment. Second, we plan to apply the optimal graph-based shortest path algorithm to simulate the 3D distribution of VCs and their aggregation characteristics. Finally, we will validate the wind speeds under the corresponding wind directions and spatial resolutions using a CFD software to assess the reliability of the simulation results.

2. Materials and methods

2.1. Study area and data

This study utilized the building contour data from the Hong Kong Lands Department (https://data.gov.hk/sc/). This dataset shows permanent buildings or structures in the entire Kowloon Peninsula in Hong Kong (Fig. 1), including building footprints, building types, building names, and building heights. The Kowloon Peninsula covers an area of about 16 km^2 and the topography is mainly flat. This area exemplifies a high-density, compact urban form, with most of its land occupied by high-rise buildings and limited urban green spaces across the study area. The concentration of tall buildings along the coastline is considered to form a ‘wall effect’. This effect impedes the flow of sea breezes and hinders ventilation throughout Kowloon (Peng et al., 2017). The Kowloon area has experienced significantly reduced ventilation due to increased building density and height (Peng et al., 2018). Combined with high temperatures and the wall effect, the urban heat island effect is pronounced in this area (Nichol et al., 2009; Yee and Kaplan, 2022).

The topography of the study area is relatively flat and can be approximated as a plane. Therefore, we standardized the urban space by converting the building shapefile into raster format at spatial resolutions of 30, 50, and 100 m. The corresponding average building heights at these resolutions were calculated as 41.79, 41.48, and 41.23 m, respectively. Based on these values, we set the upper boundary of the study area at 60 m to examine urban ventilation below this height.

Using the height attribute, we constructed a uniform 3D space to represent the city, where all dimensions have consistent lengths and units. In terms of data structures, this is a 3D array where values represent buildings. Building this 3D model is not just for data processing. As high-density areas like Kowloon in Hong Kong have significant building height differences. Only a 3D model can accurately capture how airflow climbs and bypasses these vertical obstacles. This vertical perspective is essential for reliable urban

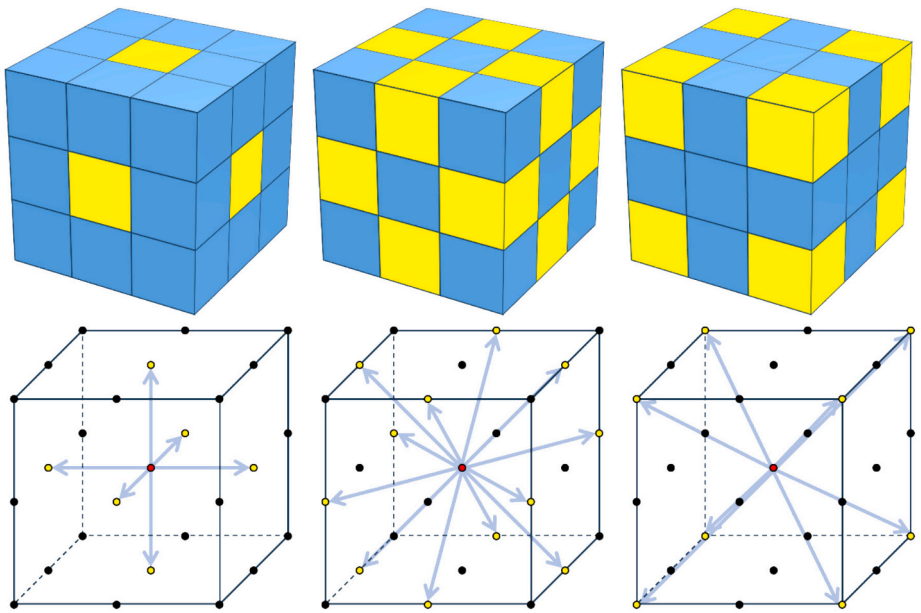

Fig. 2. The movement patterns scheme. From left to right: cube-face (1), cube-edge ($\sqrt{2}$), and cube-vertex ($\sqrt{3}$). Top: voxel patterns. Bottom: corresponding directions from the central voxel.

ventilation analysis.

2.2. Weighting strategy for LCP

In the 3D urban graph, the weights between voxels determine the cost calculation, shaping the form of the LCP. In graph-based shortest path algorithms, the cost associated with each edge represents the difficulty or resistance of moving from one voxel to the next. The algorithm calculates the shortest path by minimizing the accumulated weights along the way. The lower the weight, the more favorable the path. We assign non-passable property to building voxels. Buildings will not act as nodes and no edge will connect to them. This was done to ensure that the VCs cannot penetrate buildings and to minimize passing through building neighborhoods. The remaining voxels were defined as atmosphere, with weights significantly lower than the aforementioned type. As we wanted the VC to move freely and selectively within 3D urban space.

2.3. Graph-based movement patterns

We defined two movement patterns based on the spatial adjacency of voxels. If a voxel considers only the adjacent cube faces, we define this as a 6-direction pattern. If it also considers cube faces, cube edges, and cube vertices, we define this adjacency as a 26-direction pattern. In the graph, these movement patterns are abstracted as edges between vertices. Based on solid geometry, we set weight coefficients to determine the weight adjustment values for different movement patterns. The weights of all edges are multiplied by their corresponding coefficient. For the 6-direction pattern, the weight coefficient on edges is always 1. For the 26-direction pattern, the six cube-face coefficients are 1, the twelve cube-edge coefficients are $\sqrt{2}$, and the eight cube-vertex coefficients are $\sqrt{3}$. The schematic diagram of the movement patterns is shown in Fig. 2.

2.4. Graph-based 3D ventilation corridors simulation algorithm

When studying VCs, we need to find optimal paths in complex 3D urban spaces. This requires avoiding buildings and high resistance areas while choosing the direction of least resistance. Graph-based shortest path algorithms are well suited for identifying low-cost paths in urban environments. They progressively explore paths in a network of connected nodes and dynamically update path costs (Brandes, 2008; Fang et al., 2021; Nevat and Adelia, 2023). Several factors should be considered when selecting a shortest path search algorithm, such as the size of the graph, the presence of negative edge weights, and the necessity of a specific shortest path. Therefore, we employed three graph-based shortest path algorithms to search and estimate VCs in this study, including Dijkstra (Dijkstra, 2022), Bellman-Ford (Pramudita et al., 2019) and A* algorithm (Hong et al., 2021).

Specifically, the Dijkstra algorithm is effective in solving the shortest path problem in graphs with non-negative edge weight. The basic principle is to select the vertex with the shortest current distance to expand. The algorithm then dynamically updates the shortest path to other unvisited vertices. Bellman-Ford algorithm can handle graphs with negative edge weights but is less efficient. It is applicable to situations where the path needs to pass through high-cost areas or bear negative weight penalties, as well as dynamically varying edge weights. The A* (A-star) algorithm adopts heuristic functions such as the Euclidean distance. It can estimate the cost from the current node to the target before the path searching, improving the efficiency of goal-oriented search. Although the A* algorithm requires that all edge weights be non-negative, it significantly improves computational efficiency by using a reliable estimation rule to guide the search. The time complexity of Dijkstra algorithm, Bellman-Ford algorithm and A* algorithm can be represented as $O(E + VlogV)$, $O(V \bullet E)$, and $O(E)$, respecitvely. Where O(…) denotes the asymptotic upper bound of the algorithm's running time. V is the number of vertices and E is the number of edges in the graph. In the analysis that follows, we will compare the running times of three algorithms and select the optimal one.

2.5. Validation

Airflow Analyst was developed to utilize geospatial data such as building structure and terrain to simulate and visualize wind flow in complex urban environments (Irie, 2022; Natsume, 2019). Input parameters for Airflow Analyst calculation include building footprints and heights for constructing 3D city geometry, and 3D grid resolution for determining model accuracy. Building data

Table 1
Airflow analyst configurations.

Calculation code	RIAM-COMPACT (RC-GIS) for City
Turbulence model	Large eddy simulation
Analysis method	Transient analysis
Discretization	Difference method
Scheme	Interpolation method
Inlet boundary condition	Created by interpolation from power law or weather model
Outlet boundary condition	Convective condition
Object scan method	Extrude
Convergence test	RMS error $=1.0\ E^{-3}$, or repetition maximum 100
Resistivity model	Consider as external force term

includes detailed attributes such as building contours and heights. As described in Section 2.1, this data was rasterized at 30, 50, and 100 m spatial resolutions to normalize the simulated urban form. Airflow Analyst employs the Large Eddy Simulation (LES) technique to enable the prediction of detailed turbulence patterns (Monari and Strachan, 2017). For Airflow Analyst, the LES model that is applied is the standard Smagorinsky model. The model is conducted in a time-dependent manner, allowing the behavior of the wind over time to be visualized (Uchida and Araya, 2021). This approach has been validated by wind tunnel experiments, ensuring the accuracy of its simulation of the wind environment.

Airflow Analyst uses geographical coordinates-based grid creation to model urban areas. It performs fluid calculations that leverage multi-core central processing units (CPUs), with the option of using graphics processing units (GPUs) for enhanced performance. Airflow Analyst provides a 3D visualization of simulation results and allows users to extract numerical data at specific points or throughout the entire grid range. This feature facilitates an understanding of airflow patterns and their interaction with urban structures. Airflow Analyst has become an effective tool for analyzing ventilation, assessing turbulence risks, and understanding material dispersion in complex urban area through the above characteristics. The CFD analysis configurations are presented in Table 1. The Airflow Analyst output represents the average wind speed. To ensure comparability, four initial wind directions are used, including west to east, east to west, south to north, and north to south. This setup is consistent with the setup of the 3D LCP experiment, and matched the spatial resolution in all 3D dimensions. The wind direction setup also aims to enhance computational efficiency and avoid redundant construction of 3D voxel grids. It incorporates the most prevailing wind direction components across different seasons in Hong Kong. In this study, a comprehensive assessment of all orthogonal wind directions yields more compelling results than analyzing a single prevailing wind direction. Relying solely on a seasonal prevailing wind is insufficient for robust analysis of complex urban environments. Consequently, this study considered how varying wind directions influence the design of VCs, enabling adaptation to different seasons and coastal wind conditions. The Airflow results were exported by each z-layer, corresponding directly with the z-layers of the 3D LCP, allowing for a voxel-to-voxel comparison. For quantitative analysis, we extracted the airflow values along the major VCs and compared them with the average wind speed of each corresponding layer.

2.6. Hardware and software specifications

All simulations were performed on a high-performance workstation to maintain consistency in runtime evaluation. The processors of the workstation used are two Intel Xeon Gold 5118 CPU at 2.30 GHz. The installed RAM is 320 gigabytes. To ensure consistency between the comparison of different models, all simulations were performed in the same Python environment. Our 3D LCP implementation is based primarily on the igraph library, a powerful and efficient graph analysis toolkit that supports the rapid construction, traversal, and optimization of large-scale graphs. The igraph library provides built-in support for various shortest path algorithms and is well suited for working with complex 3D spatial data structures. All tests were executed under the same hardware configuration and operating procedures to maintain consistency in runtime performance evaluation and ensure the reliability of the comparison results. We performed the CFD validation using Airflow Analyst version 2.1.0.2, which can be seamlessly integrated into the ArcGIS platform.

3. Results

3.1. Algorithms comparison & single 3D LCP scenario

We evaluated the performance of three graph-based shortest path algorithms, namely Dijkstra, Bellman-Ford, and A*, by measuring their runtime at a spatial resolution of 100 m (Table 2). Additionally, we applied these algorithms across vertical layers within the study area and recorded their runtime at three different spatial resolutions (Table A1). The results consistently demonstrate that the Dijkstra algorithm outperforms the other two under all tested conditions. Therefore, Dijkstra was selected as the primary algorithm for subsequent analyses. This algorithm has been shown to possess universal optimality (Haeupler et al., 2024). It means that Dijkstra's algorithm achieves optimal performance in any case, regardless of the complexity of the graph. For situations without negative edge weights, the Dijkstra algorithm is usually the optimal choice, as it not only guarantees finding the shortest path but also has relatively

Table 2
Algorithms runtime comparison at 100 m spatial resolution.

Algorithm	Direction	Total paths attempted	Runtime (s)
Dijkstra	WE	58,560	23.7
Dijkstra	EW	58,560	
Dijkstra	NS	88,128	
Dijkstra	SN	88,128	
Bellman-Ford	WE	58,560	25.2
Bellman-Ford	EW	58,560	
Bellman-Ford	NS	88,128	
Bellman-Ford	SN	88,128	
A*	WE	58,560	1241.1
A*	EW	58,560	
A*	NS	88,128	
A*	SN	88,128	

low computational complexity. Additionally, its dynamic updating feature makes it particularly suitable for path planning in changing scenarios.By progressively expanding in this way, the algorithm ensures that each step selects the optimal path, ultimately guaranteeing the globally optimal path from the start to the target (Seegmiller and Shirabe, 2022).

We then conducted single 3D LCP trials within a selected subregion of the study area to clearly visualize the travel pattern of a single path. The depth, height, and width of the subregion 3D space were set to 30 m. In the trials in this section, building voxel weights were assigned a value of 128, while the weights of building neighbor voxels were set to 64. The remaining atmospheric voxels were assigned random values between 1 and 2. This hypothetical setup was intended to encourage the 3D LCP to bypass buildings and ensure that each movement step accumulates a weight greater than 1. The start point was set at a randomized point on the west side of the study area and the end point was set at a randomized point on the east side so that we could observe the 3D LCP traveling through the city.

From Figs. 3 and 4, we can see that the 3D model of the study area has been constructed, with three types of urban voxels forming the entire urban 3D space. The light gray voxels represent buildings. The outer wrapped transparent dark gray voxels represent the building neighbors. The transparent light gray voxels in the air represent the atmosphere. The red voxels represent the single path. The 3D LCP algorithm, given a specified start and end point, actively selected an optimal path. The start height is set to half the height of the 3D space and the end height is set to the first layer. This path bypassed the buildings as well as their neighbor voxels and accumulated the minimum weight to reach the set destination. Whether it is a 6-direction or a 26-direction movement pattern, the overall direction and trend are similar when viewed from the perspective of the entire urban space.

More specifically, from Fig. 5 we can see how the connectivity patterns we set up. These patterns reflected the path selection of Dijkstra's algorithm under the weighted graph, which empowered VCs to avoid high resistance and choose low resistance in urban areas. For the 6-direction pattern, we define a simple behavior pattern that allows the path to make a 90-degree turn in any direction. For the 26-direction pattern, the path can choose more directions by vertices, edges, and faces, and therefore the results are more reliable. With the same number of voxels, the 6-direction pattern greatly reduces the number of edges in the graph and saves computational speed. Specifically, in the examples in this section, the number of voxels of the graphs is 598,500, and the number of network edges for the 6-direction pattern and the 26-direction pattern are 3,499,200 and 14,739,772, respectively. Under the same computer configuration, the computation time for the 26-direction one is eventually 3.142 times longer than that for the 6-direction one.

3.2. *Multiple LCP scenario*

To represent the ventilation environment of the whole Kowloon Peninsula and the spatial patterns of the major VCs, we voxelized the whole Kowloon Peninsula as well as its airspace and then constructed a 3D urban graph. We first resampled the study area into three dimensional raster with horizontal resolution of 30 m, 50 m and 100 m. For vertical resolution, in order to more accurately reflect the bypass behavior of the 3D LCP in the high-density urban area of Kowloon Peninsula, we set the resolutions to 3 m, 5 m, and 10 m, respectively. Thus, the number of corresponding layers from vertical directions is 20, 12 and 6, respectively. We can see the basic configuration of 3D urban space under multiple 3D LCP scenarios in Table 3.

For the 3D LCP, since each atmospheric voxel in the 3D urban space is visited, we assume that in multiple LCP scenarios, the areas with the highest number of visits represent the desired VCs. To identify the major VCs, the paths were first classified into 1000 intervals

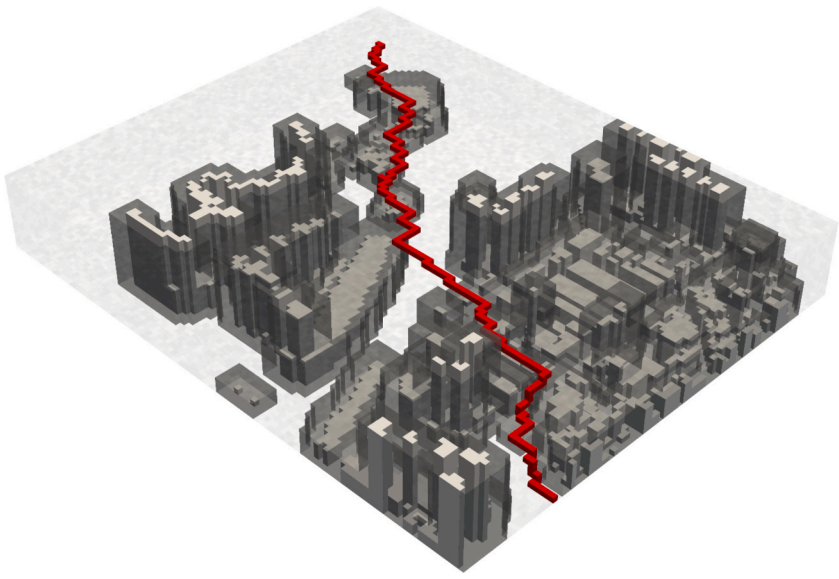

Fig. 3. Single 3D LCP schematic with 6-direction pattern.

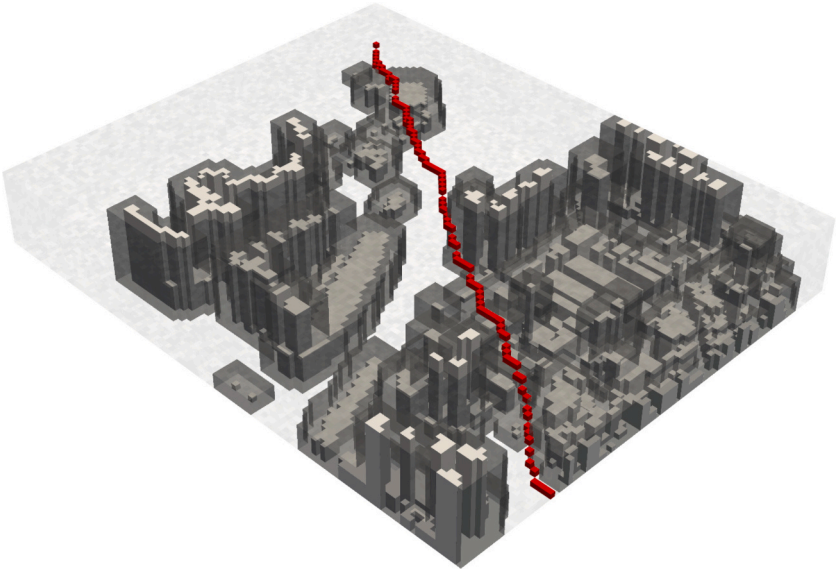

Fig. 4. Single 3D LCP schematic with 26-direction pattern.

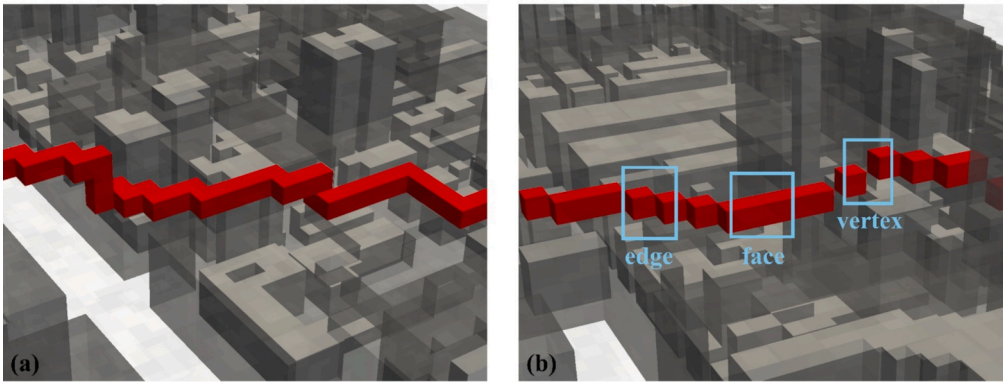

Fig. 5. Voxel connectivity schemes for single 3D LCP modeling: (a) Connectivity pattern of the 6-direction pattern. (b) Connectivity pattern of the 26-direction pattern.

Table 3
Descriptive configuration of 3D urban space.

Horizontal resolution	Vertical resolution	Layer (k)
30 m	3 m	20
50 m	5 m	12
100 m	10 m	6

using the equal breaks method based on the number of visits, and the top 1% with the highest visit frequency were selected as the major VCs. This is to exclude the effect of differences in the path count due to resolution on the selection of major VCs. Figs. 6–8 demonstrate the major VCs in different directions ranked by accumulated unique non-repeating visits under different spatial resolutions, with different building levels distinguished by color. These visualizations highlight the following key insights: as shown in Fig. 6, under the 100-m resolution, the spatial shapes and locations of the major VCs remain largely consistent in both vertical and horizontal directions. Only minor differences are observed near the starting and ending faces, which are attributed to the influence of wind direction. Fig. 7 illustrates the results at the 50-m resolution. The major VCs from west to east are generally similar in location to those at 100 m (Fig. 6), while the east-to-west paths show a noticeably straighter trajectory. The north-to-south and south-to-north directions also exhibit significant differences compared to the coarser resolution. In particular, the south-to-north direction displays a separated structure, with the major VCs splitting into two distinct paths rather than forming a single consolidated corridor. In Fig. 8, the east–west direction at the 30-m resolution closely resembles that of the 50-m case (Fig. 7). However, there is a big shift in the position of the west-to-east

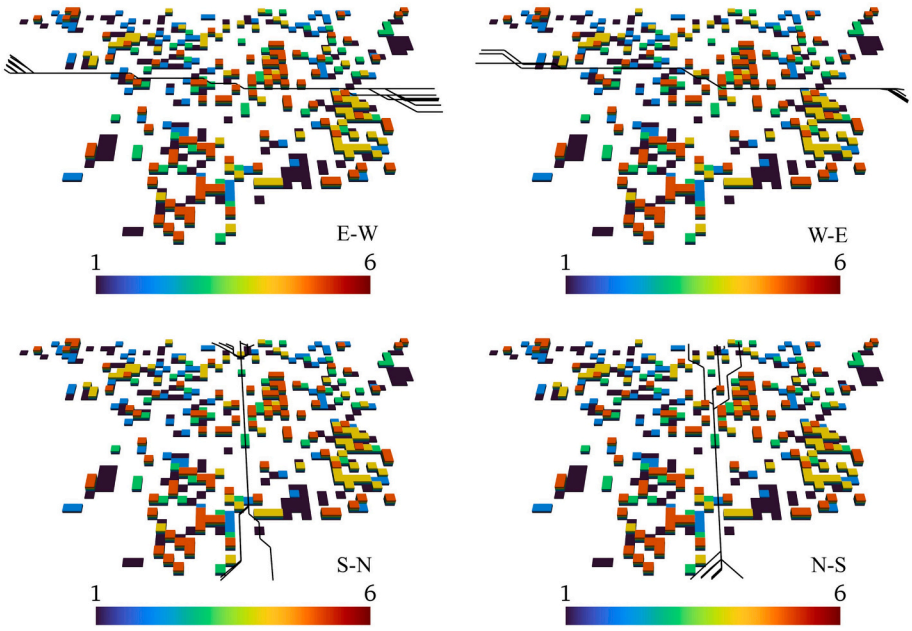

Fig. 6. Major VCs at 100 m resolution ranked by accumulated visits. The color bar indicates different vertical layers, from the bottom (1) to the top (6).

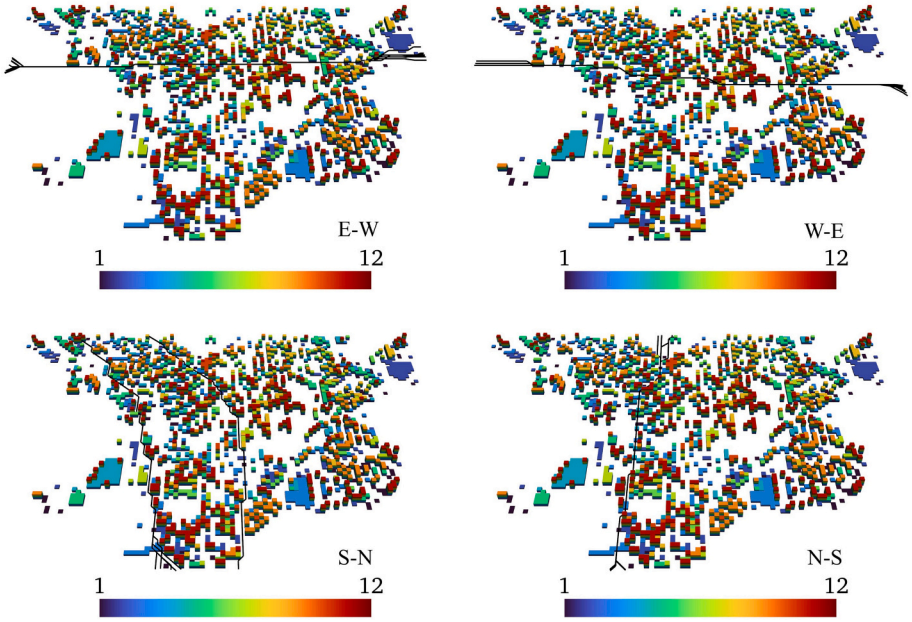

Fig. 7. Major VCs at 50 m resolution ranked by accumulated visits. The color bar indicates different vertical layers, from the bottom (1) to the top (12).

paths, indicating that the major VCs pass from the southern to the northern part of Kowloon. Both the south-to-north and north-to-south directions tend to circumvent the high-density central area in northern Kowloon, forming paths that avoid this congested zone. Major VCs naturally exhibit higher wind speeds because they represent the paths of least airflow dynamic resistance. When airflow enters a high density urban area, buildings block its movement. The air converges into these continuous open channels which will creates a channeling effect that significantly accelerates the wind. Moreover, the structural differences among VCs relate to resolution and wind direction. Coarse resolutions like 100 m tend to average the physical blocking effects of individual buildings. This allows the algorithm to identify macroscopic and dominant airflow channels. Finer resolutions like 30 m capture much more local

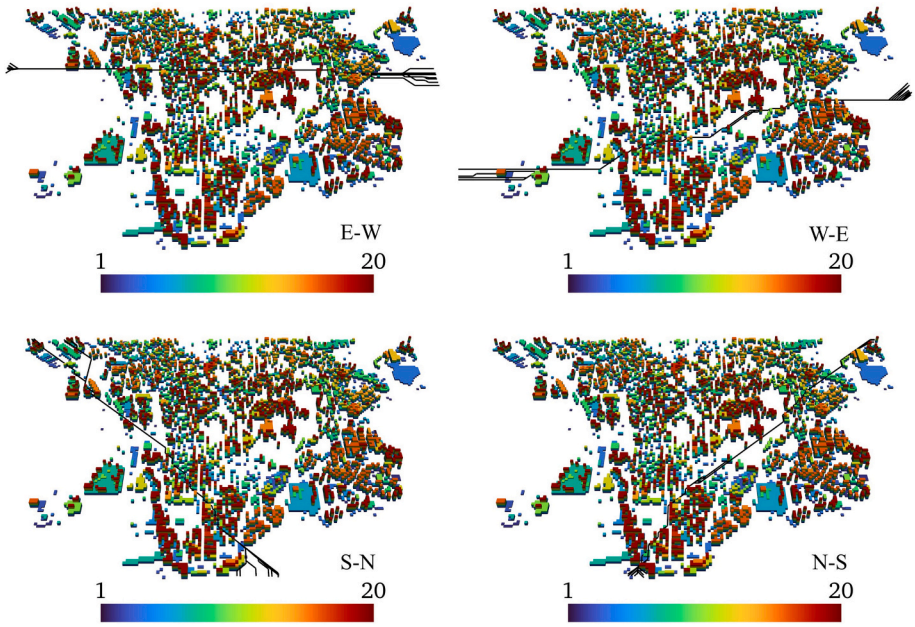

Fig. 8. Major VCs at 30 m resolution ranked by accumulated visits. The color bar indicates different vertical layers, from the bottom (1) to the top (20).

surface resistance and complex building geometries. This forces the airflow to make more localized detours when seeking the path of least resistance. Furthermore wind direction directly determines the frontal area of urban obstacles. This fundamentally alters the resistance distribution and shapes the final VCs. As spatial resolution becomes finer, the computational cost for identifying ventilation corridors increases substantially, with runtime rising from 23.7 s for 100-m resolution to 846.6 s for 50 m, and exceeding 26,590 s for 30-m resolution (Table 4).

3.3. Ventilation capacity of major VCs

Using Airflow Analyst, we conducted comprehensive CFD simulations to analyze the average wind speed across the study area, leveraging its advanced computational capabilities to model airflow dynamics in urban environments with varying spatial resolutions and complex geometries. We used the same number of grids as in Table 4 to complete the simulation of average wind speeds at the corresponding resolutions (30 m, 50 m, and 100 m). The outputs included average wind speed visualizations across multiple z-layers. Fig. 9 presents the layer-by-layer CFD simulation results at 100 m resolution, with red pixels representing areas of high wind speed and blue pixels indicating areas of low wind speed. CFD simulation results at 50 m and 30 m resolution are provided in the Appendix (Figs. A1, A2). The resolution significantly influenced the granularity of the results, with finer resolutions (30 m) providing more detailed spatial patterns of wind distribution compared to coarser resolutions (100 m).

The average wind speeds within the major VCs were analyzed across three different spatial resolutions as well as four different wind directions. Fig. 10 shows the schematic diagram of the comparison between the 3D LCP simulation results and the CFD simulation results at 100 m resolution. Schematic diagrams at 50 m and 30 m resolution are provided in the Appendix (Fig. A3, A4). Table 5

Table 4
Configuration and running parameters of the multiple 3D LCP.

Resolution	Direction	Total paths attempted	Width (voxels)	Height (voxels)	Depth (voxels)	Runtime (s)
	WE	58,560				
	EW	58,560				
	NS	88,128				
100 m	SN	88,128	54	41	6	23.7
	WE	964,320				
	EW	964,320				
	NS	1,679,616				
50 m	SN	1,679,616	108	82	12	846.6
	WE	7,110,040				
	EW	7,110,040				
	NS	10,851,984				
30 m	SN	10,851,984	179	134	20	26,590.4

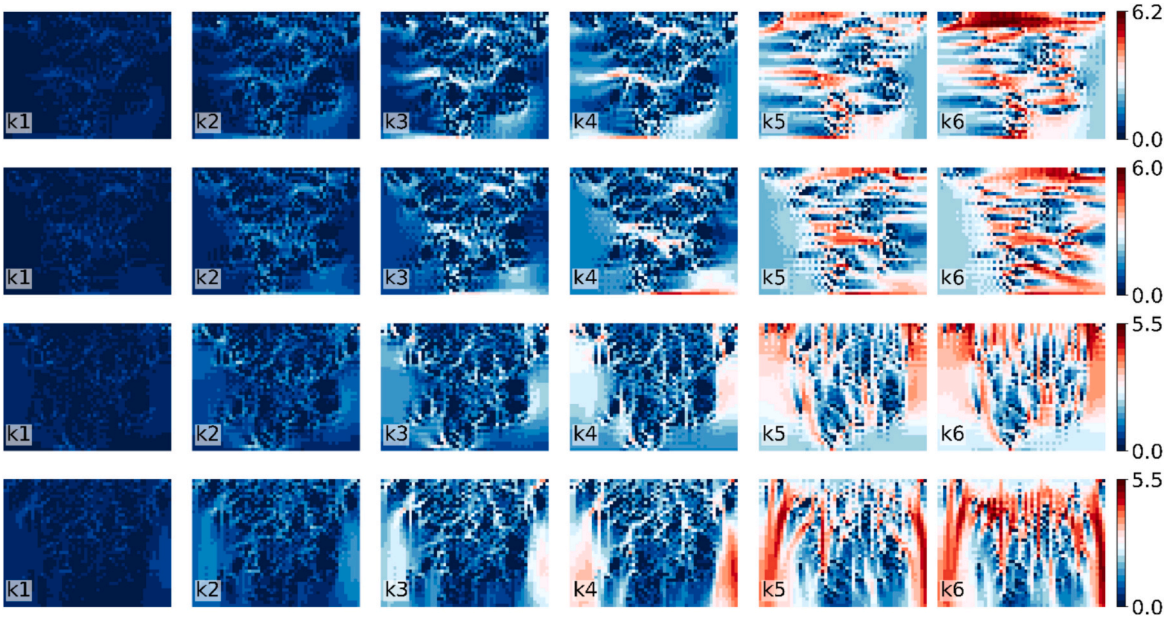

Fig. 9. Layer-by-layer wind speed simulations results of Airflow Analyst at 100 m resolutions. From top to bottom: *E*-W, W-E, S—N, N-S. The colorbar on the right of each row indicates wind speed (in m/s).

summarizes the results, revealing how wind speeds vary among these major VCs at different resolutions and wind directions and the comparison with the global wind speeds for the same conditions.

Across all wind directions, the average wind speed within Major VCs consistently exceeded the corresponding global average wind speed at all spatial resolutions. At 100 m resolution, the VCs average wind speed was 2.7160 m/s, compared to the global average wind speed of 1.4011 m/s. This difference shrank at 50 m, where the VCs average wind speed rose to 2.8179 m/s while the global mean reached around 2 m/s. However, at 30 m resolution, both VCs and global averages declined to 1.8706 m/s and 1.7429 m/s, respectively. These results suggest that a coarser spatial resolution (100 m) is more effective for identifying high-efficiency ventilation corridors, as it preserves large-scale flow patterns and amplifies the contrast between corridors and background wind fields. In contrast, finer resolutions such as 50 m and 30 m incorporate more detailed building-level interactions, which introduce localized turbulence and resistance, thereby reducing the relative wind speed advantage of VCs over the global average. When analyzing by wind directions, the W-E direction exhibited the highest average wind speed within VCs, reaching 3.0163 m/s, 3.7302 m/s, and 1.8814 m/s at 100 m, 50 m, and 30 m resolutions, respectively. The largest difference between VC and global wind speeds also occurred in the W-E direction at 50 m, where VCs wind speed (3.7302 m/s) exceeded the global average (2.0342 m/s) by 1.696 m/s. This indicates that under prevailing W-E flows, the urban morphology supports the formation of strong, concentrated ventilation corridors. In contrast, S—N and N-S directions consistently exhibited lower wind speeds in both VCs and global contexts, reflecting greater obstruction.

As can be seen in Fig. 11 a-d, the frequency histograms reveal how wind speed distributions vary with spatial resolution and wind direction across different vertical layers. At 100 m resolution, wind speeds are predominantly concentrated within a narrow low-speed range across all directions, with distributions showing relatively uniform patterns between layers. As the resolution increases to 50 m, the frequency distributions become more dispersed, with noticeable increases in mid-range wind speeds. This trend is particularly evident in the S—N and W-E directions. At 30 m resolution, the histograms display the broadest range of wind speeds, with multiple layers showing substantial frequencies in higher-speed intervals. Finer resolutions such as 30 m can capture more local turbulence and structural channel effects, thereby resulting in greater vertical airflow variations. Among all directions, S—N and N-S exhibit the widest and most layered wind speed distribution, while wind speeds in the W-E and *E*-W directions are more skewed toward lower speeds. These patterns support the view that both resolution and wind direction affect the spatial structure of urban wind flow. Furthermore, a more refined grid will enhance the detection of stratified and direction-sensitive VCs.

The results in this section indicate that major VCs consistently outperform the overall wind environment across all resolutions and directions. On average, wind speeds within VCs are 1.43 times higher than the global average, confirming their role in enhancing airflow. At a resolution of 100 m, the major VCs shows the greatest advantage over the global VCs. As resolution increases, this difference narrows, indicating that finer spatial detail may capture more localized turbulence and resistance, ultimately weakening overall ventilation efficiency. Directionally, W–E flows produce the highest VC wind speeds and greatest differences. Although the proposed 3D LCP algorithm can effectively identify 3D VCs in high-density urban environments, it still has several limitations. Our 3D LCP approach assumes a static environment. It does not account for real time atmospheric dynamics or thermal effects. Meanwhile, CFD simulations at very high resolutions can produce localized turbulence anomalies. These extreme local fluctuations might not perfectly reflect actual continuous wind fields. Consequently, our analysis targets continuous ventilation paths to avoid the influence of

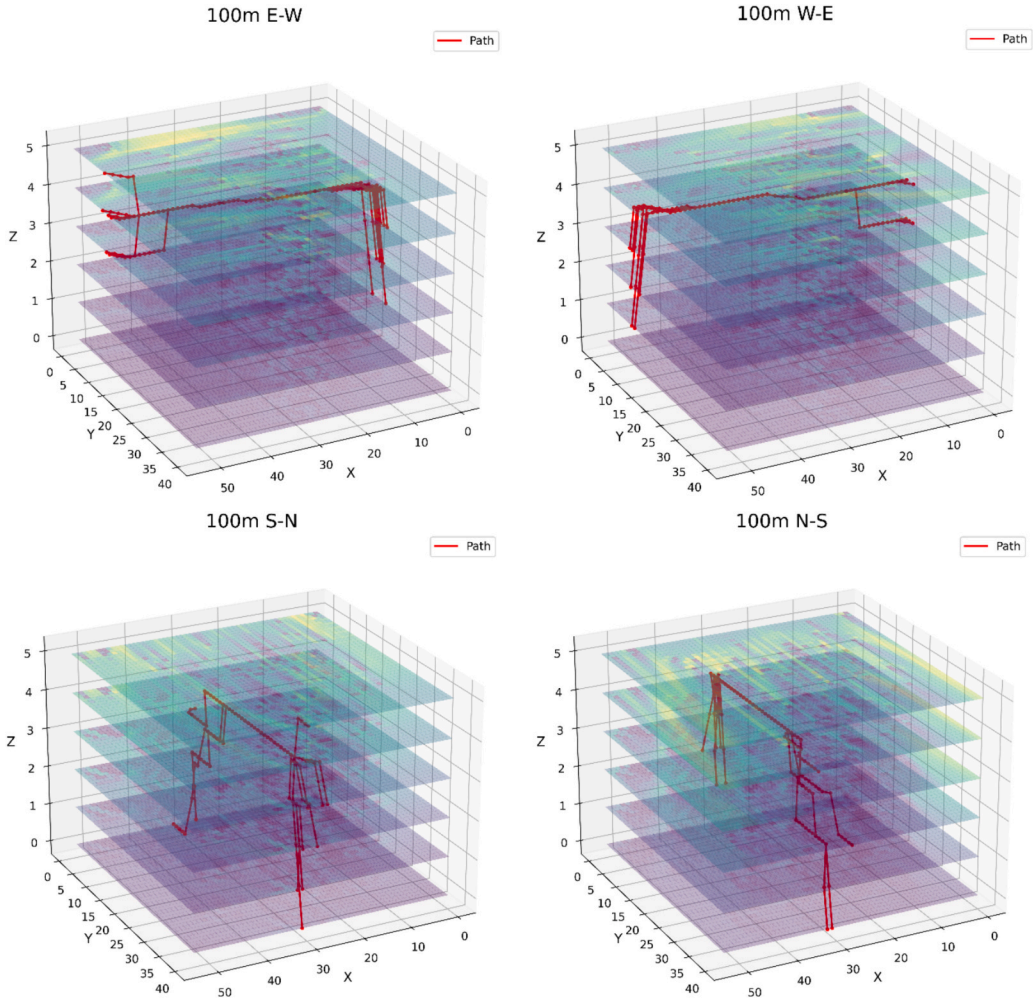

Fig. 10. Overlay of Major VCs and Airflow Analyst simulation results at 100 m resolution (The numbers on the X Y and Z axes represent horizontal and vertical voxel grid indices).

Table 5
Airflow analyst average wind speed statistical results within and outside of major VCs.

Direction	Resolution	VCs_WindSpeed (m/s)	Global_WindSpeed (m/s)
EW	100 m	3.1488	a
WE		3.0163	1.3691
SN		2.3261	1.3732
NS		2.3727	1.4632
EW	50 m	3.3011	2.0125
WE		3.7302	2.0342
SN		2.1924	1.9624
NS		2.0478	1.9963
EW	30 m	1.8395	1.7984
WE		1.8814	1.7487
SN		1.8557	1.7209
NS		1.9059	1.7037

localized wind speed variations.

4. Discussion

This study successfully applied graph-based 3D Least-Cost Path (LCP) algorithms to identify VCs in high dense urban area. We were

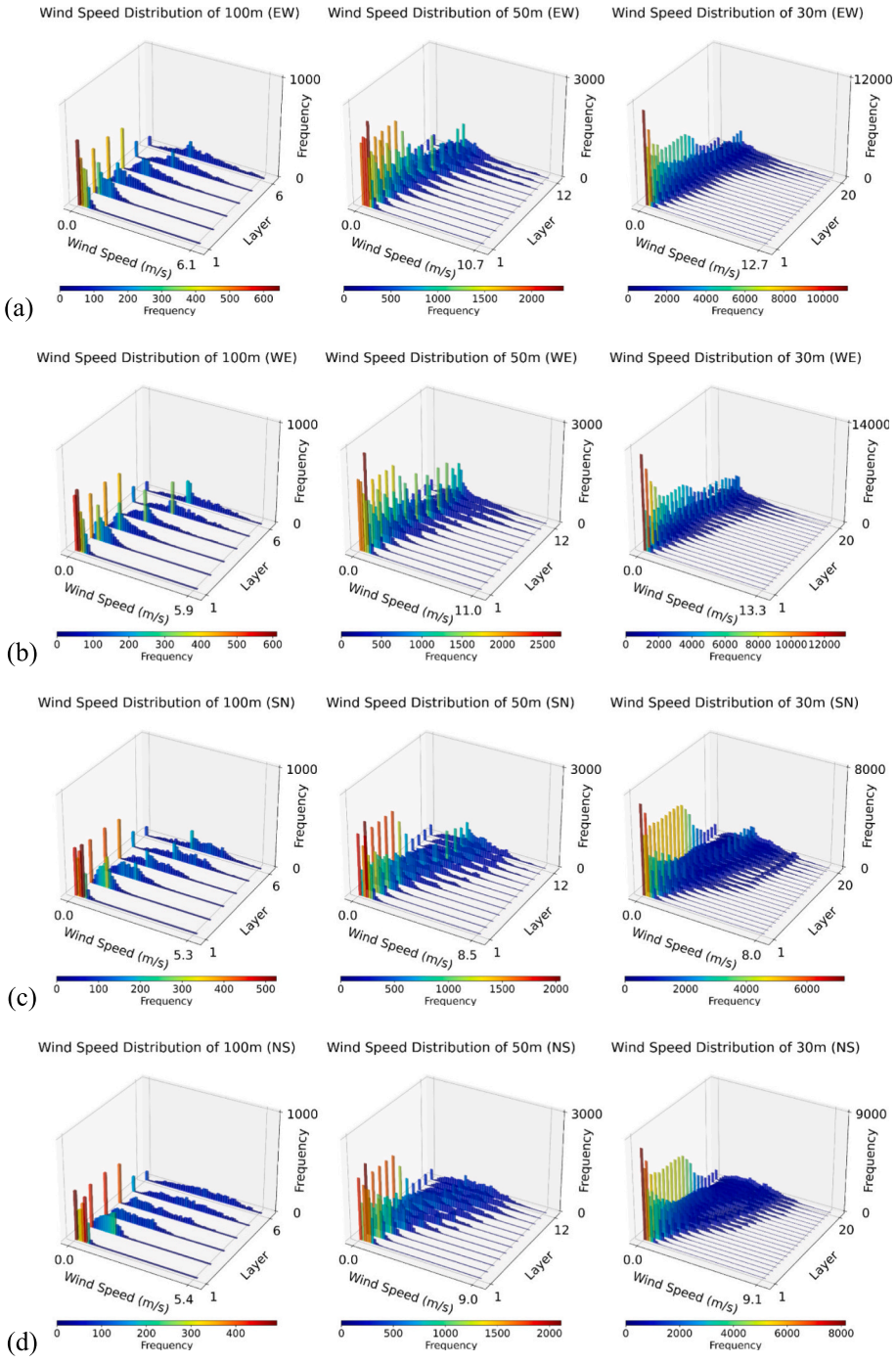

Fig. 11. Histograms of wind speed frequency distribution in different layers at three resolutions.

able to efficiently simulate single and multiple VCs by constructing voxel-based 3D urban spaces and employing the optimal algorithm. The findings demonstrate that finer spatial resolutions (e.g., 30 m) reveal more detailed airflow pathways, especially in high-density areas, while coarser resolutions (e.g., 100 m) provide a macro-scale overview of ventilation patterns. The 3D LCP method we proposed overcame the previous limitation that partially or completely ignore the depth dimension on VCs research in high-compact urban environments (Lau et al., 2024; Liu et al., 2025a, 2025b; Ying et al., 2023). In our research results, it can be observed how major VCs bypass compact and high-rise urban areas. These results show how urban morphology shape wind flow. Aligning with findings from Seegmiller and Shirabe (2022) on the importance of considering complex spatial interactions, the 26-direction movement pattern proved more effective in identifying detailed ventilation pathways compared to the 6-direction pattern.

Research results confirm that the voxel-based 3D modeling method has significant advantages, and the effect is even better when combined with the Dijkstra algorithm. This combination shows efficient computing performance and can effectively handle complex urban geometric forms. Validated by CFD simulation, the reliability of this method has been confirmed. However, this study also revealed certain limitations:

- The finer resolutions (e.g., 30 m) required significantly higher computational resources, making large-scale applications challenging.
- The exclusion of negative edge weights limited the algorithm's flexibility, suggesting that alternative methods, such as the Bellman-Ford or A* algorithm, may be required for more complex scenarios.
- The static nature of the model did not account for dynamic environmental factors like changing wind directions, real-time weather data, air temperature/pressure, aerosol and pollutants.

We also wanted to compare the capability of the 3D LCP method and the traditional 2D LCP method to explore or estimate ventilation corridors in a 3D urban space, and we set up an additional set of ideal experiments for this purpose. Using the same three spatial resolutions and four wind directions as in the main analysis, we adopted the building footprint data from Section 2.1 and segmented it according to the vertical layering scheme previously introduced. This process generated cross-sectional building layers at each height, from which we computed horizontal building density grids using square cells at each resolution. These cross-sectional building density rasters were then used as resistance surfaces to perform the same three graph-based shortest path algorithms. We compared their runtime performance and selected the optimal algorithm accordingly. After obtaining layer-by-layer LCP results, we identified the top 1% most efficient paths in each layer as the major ventilation corridors and subsequently compared their wind speeds with CFD simulation results.

Fig. 12 indicated that the wind speed within the 2D layer by layer LCP is generally greater than the global wind speed. However, the average wind speed ratio of 2D LCP to the global average is only 1.35. In some extreme cases, this ratio even drops to 1.0 or slightly lower. This means the 2D method sometimes identifies pathways with lower wind speeds than the background environment. This performance is significantly lower and less stable than the consistent 1.43 ratio achieved by our 3D LCP approach. This substantial quantitative gap implies a severe vertical level limitation of the traditional 2D method. The 2D approach fails to capture the complex vertical airflow dynamics effectively. This clearly confirms the validity and absolute necessity of the 3D LCP practice in this paper.

Future research should aim to expand the applicability of this method in several directions. First, integrating real-time and all-sky environmental data would enable dynamic modeling of ventilation corridors, allowing for adaptive simulations under varying wind and other atmospheric conditions. Second, exploring alternative algorithms, such as heuristic or hybrid models, could address limitations like negative edge weights and enhance computational efficiency, and weighting considerations still require reference to atmospheric conditions. Third, applying this approach to larger metropolitan areas or comparing results across diverse urban typologies could help generalize findings and refine the method for broader applications. This research has significant practical significance for urban planning and microclimate improvement strategies. Urban planners can enhance air circulation in high-density cities by determining the optimal VCs. Thereby effectively reducing the urban heat island effect and improving air quality. The method we proposed for determining VCs using 3D LCP can optimize the airflow and minimize hotspots and heat accumulation to the greatest extent. The 3D LCP method can also support dynamic ventilation strategies improvement, allowing city to adapt to seasonal or real-time wind direction changes. It is a potential tool for addressing the challenges brought about by rapid urbanization and climate change, and helps achieve sustainable and climate-resilient urban development.

5. Conclusions

This study demonstrated the effectiveness of the graph-based 3D Least Cost Path (LCP) algorithms in identifying Ventilation Corridors (VCs) in the compact high-rise urban environment. We provided an effective framework for simulating VCs by constructing a voxel-based 3D urban model and considering both vertical and horizontal air flow patterns simultaneously. The research results emphasized the importance of determining spatial resolution and wind direction. A finer resolution can provide more local insights. Through CFD simulation validation, at resolutions of 100 m, 50 m, and 30 m, the wind speed within VCs were 1.94, 1.41, and 1.08 times of the global wind speed respectively. These CFD results proved the advantages and effectiveness of the method we proposed.

This research can provide a potential tool for optimizing ventilation strategies, reducing urban heat islands and improving air quality. However, the demand for high-performance computing resources and limiting factors such as the simulation of small planar scenarios also point out the deficiencies. Future research should focus on integrating dynamic atmospheric environment data, exploring alternative algorithms to improve computational efficiency, and applying this method to a wider range of human habitats.

CRediT authorship contribution statement

Yifan Luo: Writing – original draft, Visualization, Validation, Software, Methodology. **Xinyu Yu:** Writing – review & editing, Supervision. **Majid Nazeer:** Writing – review & editing, Supervision. **Man Sing Wong:** Writing – review & editing, Supervision, Conceptualization. **Jinxin Yang:** Writing – review & editing. **Rui Zhu:** Writing – review & editing.

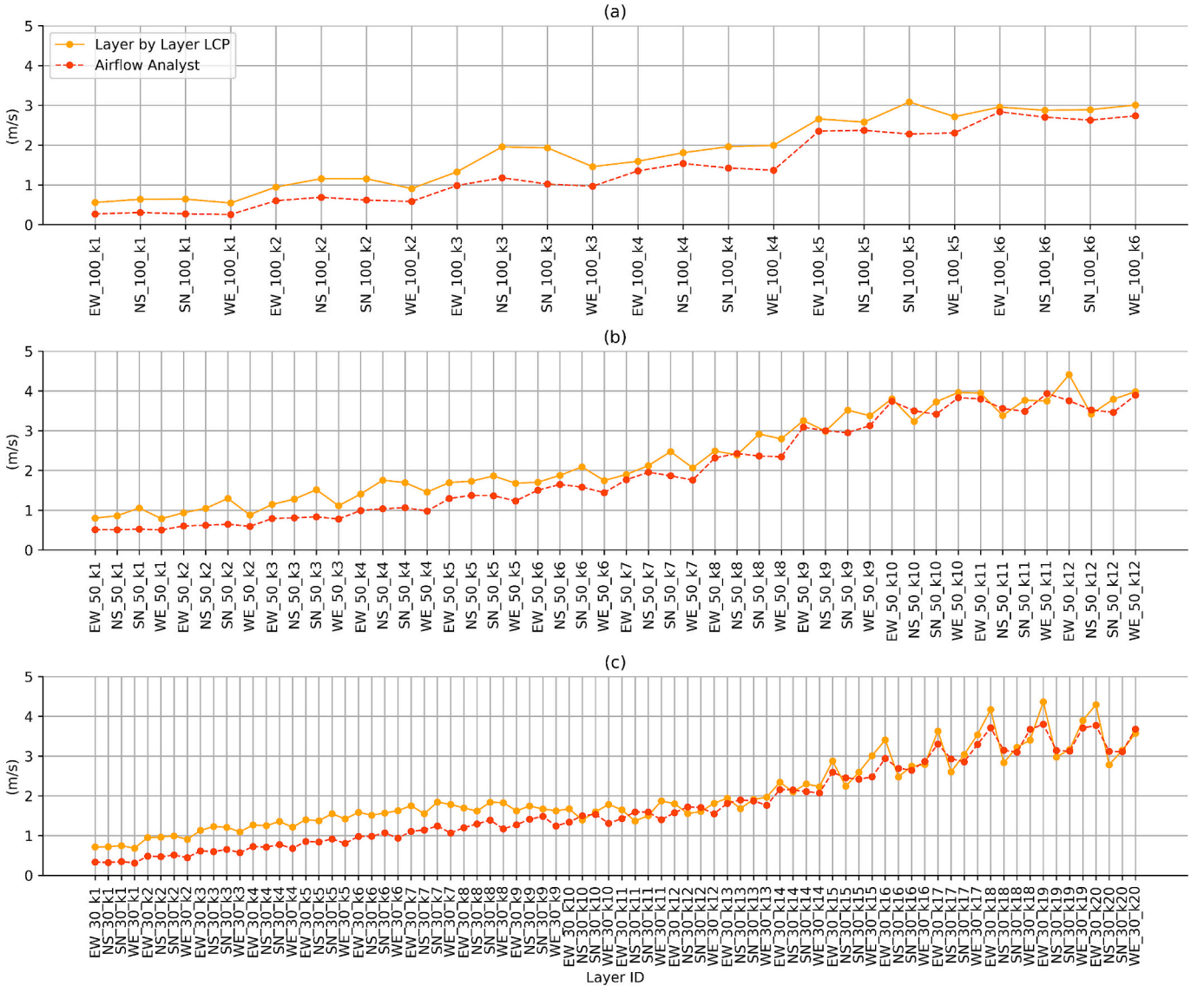

Fig. 12. Comparison of average wind speeds between Layer by Layer LCP and Airflow Analyst at three resolutions: (a) 100 m, (b) 50 m, and (c) 30 m. X-axis abbreviations denote wind direction, spatial resolution, and vertical layer index *k*.

Fundings

This project is substantially funded by the General Research Fund (Grant No. 15603923, 15609421 and PolyU15306224), and the Collaborative Research Fund (Grant No. C5062–21GF) and Young Collaborative Research Fund (Grant No. C6003—22Y) from the Research Grants Council, Hong Kong, China. The authors acknowledge the funding support (Grant No. N-ZH8S, BBG2 and 1-CDL5) from the Otto Poon Research Institute for Climate-Resilient Infrastructure, Research Institute for Sustainable Urban Development, Research Institute of Land and Space, The Hong Kong Polytechnic University, Kowloon, Hong Kong, China. This work was also supported by the State Key Laboratory of Climate Resilience for Coastal Cities at the Hong Kong Polytechnic University.

Declaration of competing interest

The authors declare that they have no known competing financial interests or personal relationships that could have appeared to influence the work reported in this paper.

Acknowledgements

The authors would like to thank the Lands Department of the Hong Kong SAR Government for providing the building contour data.

Appendix A. Appendices

Table A1. Algorithm runtime of layer by layer LCP.

Algorithm	Resolution	Direction	Total paths attempted	Runtime (s)
Dijkstra	100	WE	1680	13.3
Dijkstra	100	EW	1680	
Dijkstra	100	NS	2916	
Dijkstra	100	SN	2916	
Bellman-Ford	100	WE	1680	14.5
Bellman-Ford	100	EW	1680	
Bellman-Ford	100	NS	2916	
Bellman-Ford	100	SN	2916	
A*	100	WE	1680	241
A*	100	EW	1680	
A*	100	NS	2916	
A*	100	SN	2916	
Dijkstra	50	WE	6478	57.3
Dijkstra	50	EW	6478	
Dijkstra	50	NS	11,664	
Dijkstra	50	SN	11,664	
Bellman-Ford	50	WE	6478	63.5
Bellman-Ford	50	EW	6478	
Bellman-Ford	50	NS	11,664	
Bellman-Ford	50	SN	11,664	
A*	50	WE	6478	806.3
A*	50	EW	6478	
A*	50	NS	11,664	
A*	50	SN	11,664	
Dijkstra	30	WE	17,286	181.4
Dijkstra	30	EW	17,286	
Dijkstra	30	NS	32,041	
Dijkstra	30	SN	32,041	
Bellman-Ford	30	WE	17,286	200.5
Bellman-Ford	30	EW	17,286	
Bellman-Ford	30	NS	32,041	
Bellman-Ford	30	SN	32,041	
A*	30	WE	17,286	1657.2
A*	30	EW	17,286	
A*	30	NS	32,041	
A*	30	SN	32,041	

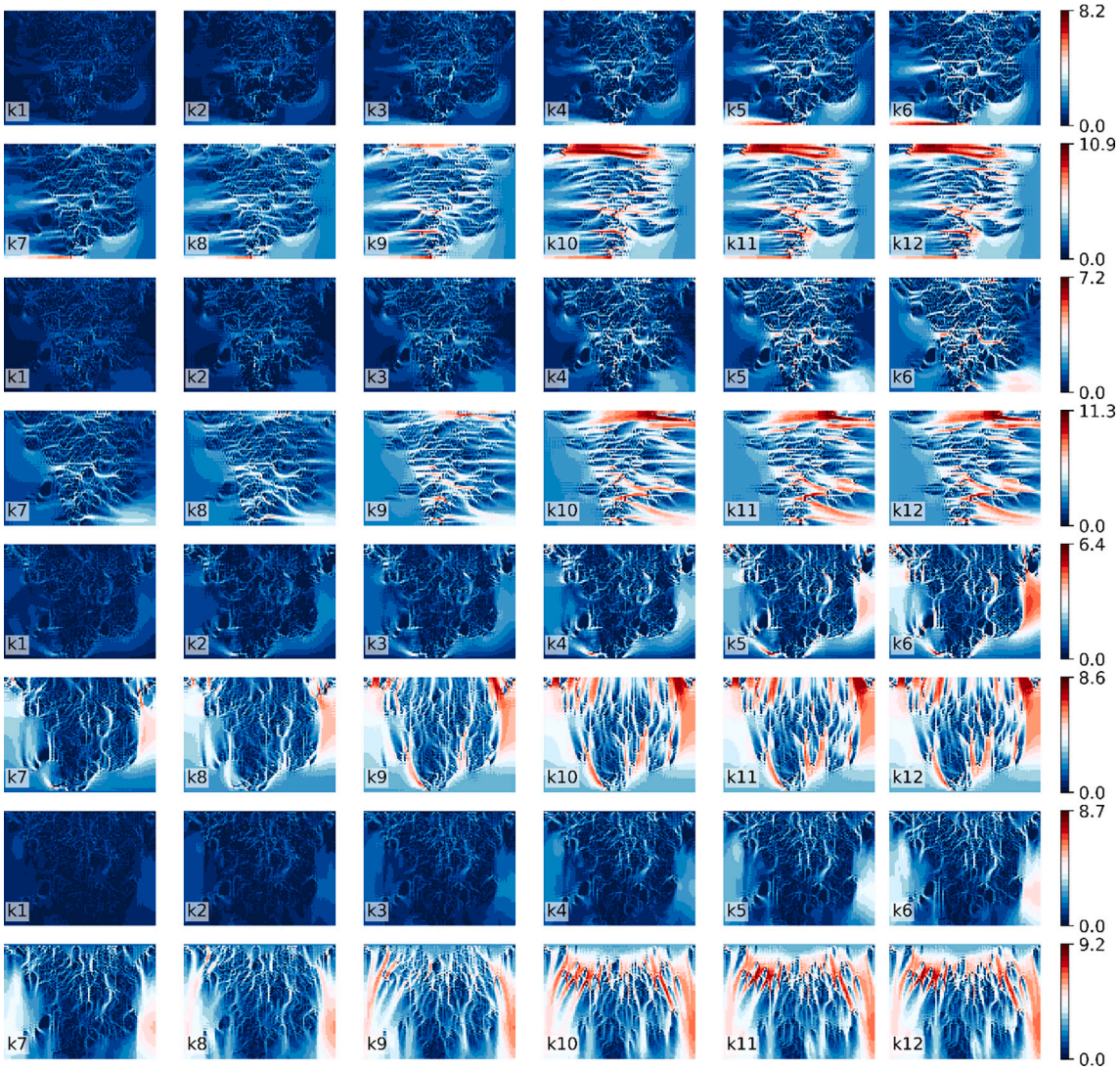

Fig. A1. Layer-by-layer wind speed simulations results of Airflow Analyst at 50 m resolutions. From top to bottom: *E*-W, W-E, S—N, N-S. The colorbar on the right of each row indicates wind speed (in m/s).

Fig. A2. Layer-by-layer wind speed simulations results of Airflow Analyst at 30 m resolutions. From top to bottom: E-W, W-E, S—N, N-S. The colorbar on the right of each row indicates wind speed (in m/s).

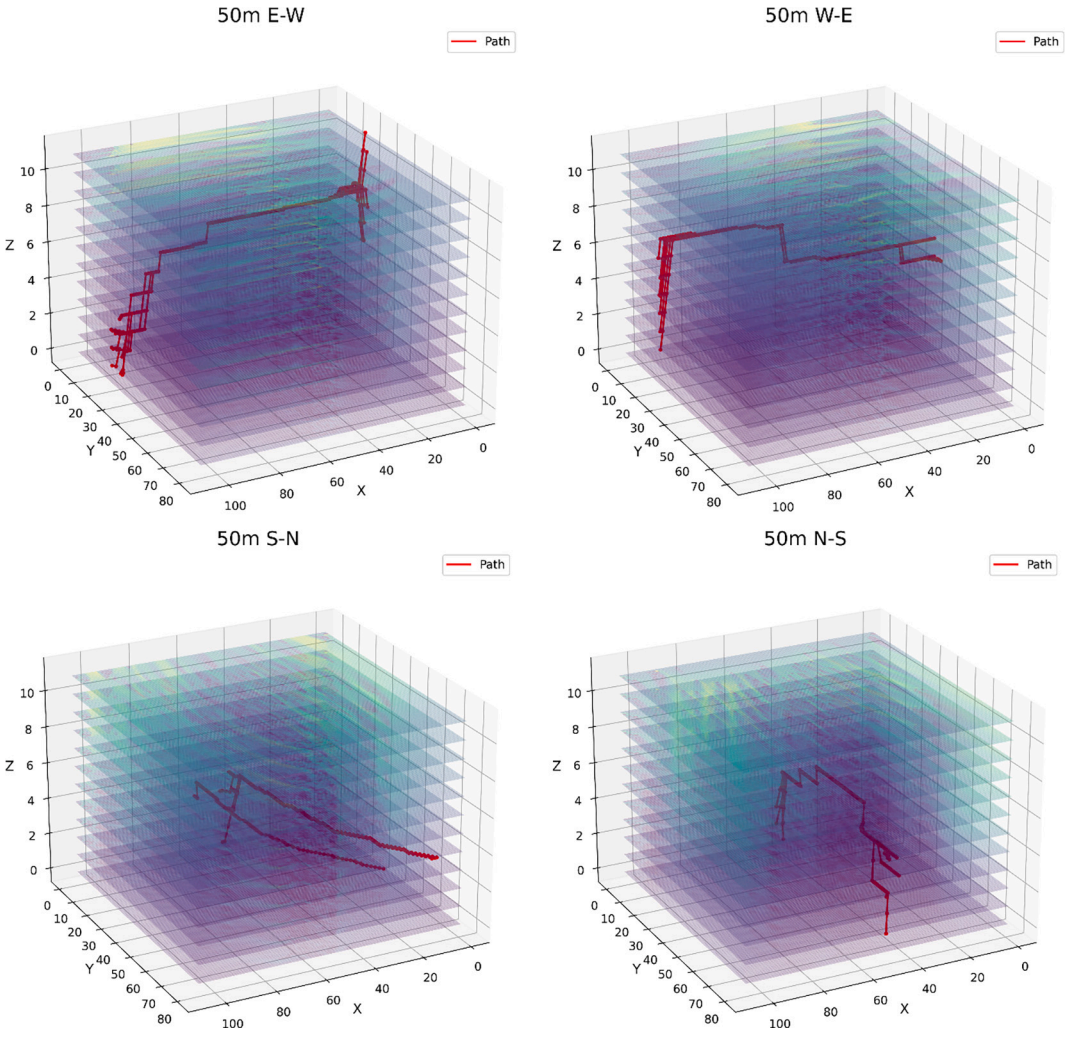

Fig. A3. Overlay of Major VCs and Airflow Analyst simulation results at 50 m resolution.

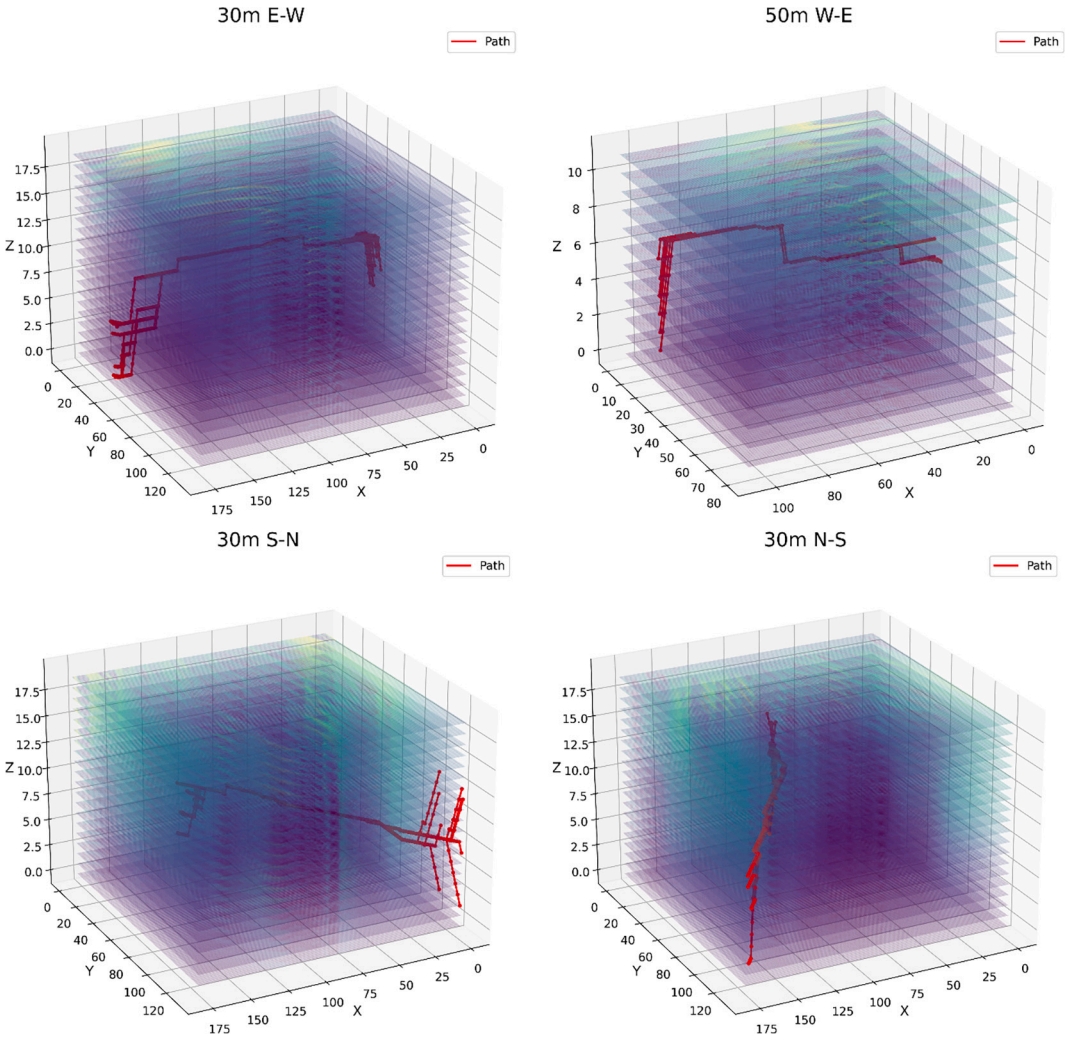

Fig. A4. Overlay of Major VCs and Airflow Analyst simulation results at 30 m resolution.

Data availability

Data will be made available on request.

References

Bady, M., Kato, S., Takahashi, T., Huang, H., 2011. An experimental investigation of the wind environment and air quality within a densely populated urban street canyon. J. Wind Eng. Ind. Aerodyn. 99 (8), 857–867. https://doi.org/10.1016/j.jweia.2011.06.005.

Brandes, U., 2008. On variants of shortest-path betweenness centrality and their generic computation. Soc. Networks 30 (2), 136–145. https://doi.org/10.1016/j.socnet.2007.11.001.

Buccolieri, R., Hang, J., 2019. Recent advances in urban ventilation assessment and flow modelling. Atmosphere *10* (3), 3. https://doi.org/10.3390/atmos10030144.

Dang, B., Liu, Y., Lyu, H., Zhou, X., Du, W., Xuan, C., Xing, P., Yang, R., Xiong, F., 2022. Assessment of urban climate environment and configuration of ventilation corridor: a refined study in Xi'an. J. Meteorol. Res. 36 (6), 914–930. https://doi.org/10.1007/s13351-022-2035-0.

Dijkstra, E.W., 2022. A note on two problems in connexion with graphs. In: Edsger Wybe Dijkstra: His Life,Work, and Legacy, 1st ed vol. 45. Association for Computing Machinery, pp. 287–290. https://doi.org/10.1145/3544585.3544600.

Fang, Y., Zhao, L., 2022. Assessing the environmental benefits of urban ventilation corridors: a case study in Hefei, China. Build. Environ. 212, 108810. https://doi.org/10.1016/j.buildenv.2022.108810.

Fang, Y., Gu, K., Qian, Z., Sun, Z., Wang, Y., Wang, A., 2021. Performance evaluation on multi-scenario urban ventilation corridors based on least cost path. J. Urban Manag. 10 (1), 3–15. https://doi.org/10.1016/j.jum.2020.06.006.

Gartland, L.M., 2008. Heat Islands: Understanding and Mitigating Heat in Urban Areas. Routledge. https://doi.org/10.4324/9781849771559.

Haeupler, B., Hladík, R., Rozhoň, V., Tarjan, R., Tětek, J., 2024. *Universal optimality of Dijkstra via beyond-worst-case heaps* (arXiv:2311.11793). arXiv. https://doi.org/10.48550/arXiv.2311.11793.

Hong, Z., Sun, P., Tong, X., Pan, H., Zhou, R., Zhang, Y., Han, Y., Wang, J., Yang, S., Xu, L., 2021. Improved A-star algorithm for long-distance off-road path planning using terrain data map. ISPRS Int. J. Geo Inf. 10 (11), 11. https://doi.org/10.3390/ijgi10110785.
Irie, T., 2022. The cooling effect of green infrastructure in mitigating nocturnal urban heat islands: a case study of Yoyogi Park and Meiji Jingu shrine in Tokyo. Landsc. Res. 47 (5), 559–583. https://doi.org/10.1080/01426397.2022.2050195.
Lau, T.-K., Tsai, P.-C., Ou, H.-Y., Lin, T.-P., 2024. Efficient and cost-effective method for identifying urban ventilation corridors using a heuristic search algorithm. Sustain. Cities Soc. 101, 105144. https://doi.org/10.1016/j.scs.2023.105144.
Liu, R., Wang, Y., Zhang, Y., Peng, Z., Chen, H., Li, X., Li, H., Li, W., 2025a. Analysis of the city-scale wind environment and detection of ventilation corridors in high-density metropolitan areas based on CFD method. Urban Clim. 59, 102274. https://doi.org/10.1016/j.uclim.2024.102274.
Liu, C., Ye, X., Huang, X., Xu, Y., 2025b. Vertical dimension of urban thermal environments: a literature survey. Cities 158, 105629. https://doi.org/10.1016/j.cities.2024.105629.
Lu, H., Guan, R., Xia, M., Zhang, C., Miao, C., Ge, Y., Wu, X., 2022. Very high-resolution remote sensing-based mapping of urban residential districts to help combat COVID-19. Cities 126, 103696. https://doi.org/10.1016/j.cities.2022.103696.
Luo, Y., Yang, J., Shi, Q., Xu, Y., Menenti, M., Wong, M.S., 2023. Seasonal cooling effect of vegetation and albedo applied to the LCZ classification of three Chinese megacities. Remote Sens. 15 (23), 23. https://doi.org/10.3390/rs15235478.
Luo, Y., Wu, Z., Wong, M.S., Yang, J., Jiao, Z., 2024. Simulating the impact of ventilation corridors for cooling air temperature in local climate zone scheme. Sustain. Cities Soc. 115, 105848. https://doi.org/10.1016/j.scs.2024.105848.
Ma, T., Chen, T., 2022. Outdoor ventilation evaluation and optimization based on spatial morphology analysis in Macau. Urban Clim. 46, 101335. https://doi.org/10.1016/j.uclim.2022.101335.
Monari, F., Strachan, P., 2017. Characterization of an airflow network model by sensitivity analysis: parameter screening, fixing, prioritizing and mapping. J. Build. Perform. Simul. 10 (1), 17–36. https://doi.org/10.1080/19401493.2015.1110621.
Montazeri, H., Blocken, B., Hensen, J.L.M., 2015. Evaporative cooling by water spray systems: CFD simulation, experimental validation and sensitivity analysis. Build. Environ. 83, 129–141. https://doi.org/10.1016/j.buildenv.2014.03.022. Special Issue: Climate Adaptation in Cities.
Natsume, M., 2019. Wind condition analysis of Japanese rural landscapes in the 19th century: a case study of Kichijoji Village in Musashino upland. ISPRS Int. J. Geo Inf. 8 (9), 9. https://doi.org/10.3390/ijgi8090396.
Nevat, I., Adelia, A.S., 2023. Urban wind corridors analysis via network theory. Atmosphere 14 (3), 3. https://doi.org/10.3390/atmos14030572.
Ng, E., Yuan, C., Chen, L., Ren, C., Fung, J.C.H., 2011. Improving the wind environment in high-density cities by understanding urban morphology and surface roughness: a study in Hong Kong. Landsc. Urban Plan. 101 (1), 59–74. https://doi.org/10.1016/j.landurbplan.2011.01.004.
Nichol, J.E., Fung, W.Y., Lam, K., Wong, M.S., 2009. Urban heat island diagnosis using ASTER satellite images and 'in situ' air temperature. Atmos. Res. 94 (2), 276–284. https://doi.org/10.1016/j.atmosres.2009.06.011.
Peng, F., Wong, M.S., Ho, H.C., Nichol, J., Chan, P.W., 2017. Reconstruction of historical datasets for analyzing spatiotemporal influence of built environment on urban microclimates across a compact city. Build. Environ. 123, 649–660. https://doi.org/10.1016/j.buildenv.2017.07.038.
Peng, L., Liu, J.-P., Wang, Y., Chan, P., Lee, T., Peng, F., Wong, M., Li, Y., 2018. Wind weakening in a dense high-rise city due to over nearly five decades of urbanization. Build. Environ. 138, 207–220. https://doi.org/10.1016/j.buildenv.2018.04.037.
Pramudita, R., Heryanto, H., Trias Handayanto, R., Setiyadi, D., Arifin, R.W., Safitri, N., 2019. Shortest path calculation algorithms for geographic information systems. In: 2019 Fourth International Conference on Informatics and Computing (ICIC), pp. 1–5. https://doi.org/10.1109/ICIC47613.2019.8985871.
Qiao, Z., Xu, X., Wu, F., Luo, W., Wang, F., Liu, L., Sun, Z., 2017. Urban ventilation network model: a case study of the core zone of capital function in Beijing metropolitan area. J. Clean. Prod. 168, 526–535. https://doi.org/10.1016/j.jclepro.2017.09.006.
Ren, C., Yang, R., Cheng, C., Xing, P., Fang, X., Zhang, S., Wang, H., Shi, Y., Zhang, X., Kwok, Y.T., Ng, E., 2018. Creating breathing cities by adopting urban ventilation assessment and wind corridor plan – the implementation in Chinese cities. J. Wind Eng. Ind. Aerodyn. 182, 170–188. https://doi.org/10.1016/j.jweia.2018.09.023.
Seegmiller, L., Shirabe, T., 2022. A method for finding least-cost corridors in three-dimensional raster space. Trans. GIS 26 (2), 1098–1115. https://doi.org/10.1111/tgis.12864.
Stewart, I.D., Oke, T.R., Krayenhoff, E.S., 2014. Evaluation of THE 'local climate zone' scheme using temperature observations and model simulations: evaluation of the 'local climate zone' scheme. Int. J. Climatol. 34 (4), 1062–1080. https://doi.org/10.1002/joc.3746.
Stott, P., 2016. How climate change affects extreme weather events. Science 352 (6293), 1517–1518. https://doi.org/10.1126/science.aaf7271.
Uchida, T., Araya, R., 2021. Applications of the atmospheric transport and diffusion of LES modeling to the spread and dissipation of COVID-19 aerosol particles inside and outside the Japan National Stadium (Tokyo Olympic Stadium). Model. Simul. Eng. 2021 (1), 8822548. https://doi.org/10.1155/2021/8822548.
Wang, H., He, P., Wong, M.S., Wong, S.W., Song, Y., Shen, G.Q., 2025. Optimizing vertical urban development: the role of a multidimensional assessment framework for balancing vertical growth and habitability. Habitat Int. 161, 103424. https://doi.org/10.1016/j.habitatint.2025.103424.
Wicht, M., Wicht, A., Osińska-Skotak, K., 2017. Detection of ventilation corridors using a spatio-temporal approach aided by remote sensing data. Euro. J. Rem. Sens. 50 (1), 254–267. https://doi.org/10.1080/22797254.2017.1318672.
Wong, M.S., Nichol, J.E., To, P.H., Wang, J., 2010. A simple method for designation of urban ventilation corridors and its application to urban heat island analysis. Build. Environ. 45 (8), 1880–1889. https://doi.org/10.1016/j.buildenv.2010.02.019.
Wong, M.S., Nichol, J., Ng, E., 2011. A study of the "wall effect" caused by proliferation of high-rise buildings using GIS techniques. Landsc. Urban Plan. 102 (4), 245–253. https://doi.org/10.1016/j.landurbplan.2011.05.003.
Yang, X., Li, Y., 2015. The impact of building density and building height heterogeneity on average urban albedo and street surface temperature. Build. Environ. 90, 146–156. https://doi.org/10.1016/j.buildenv.2015.03.037.
Yee, M., Kaplan, J.O., 2022. Drivers of urban heat in Hong Kong over the past 116 years. Urban Clim. 46, 101308. https://doi.org/10.1016/j.uclim.2022.101308.
Ying, S., Wang, M., Zhang, W., Sun, H., Li, C., 2023. City-scale ventilation analysis using 3D buildings with Guangzhou case. Urban Clim. 49, 101471. https://doi.org/10.1016/j.uclim.2023.101471.
Yuan, C., Ng, E., 2012. Building porosity for better urban ventilation in high-density cities – a computational parametric study. Build. Environ. 50, 176–189. https://doi.org/10.1016/j.buildenv.2011.10.023.
Zahid Iqbal, Q.M., Chan, A.L.S., 2016. Pedestrian level wind environment assessment around group of high-rise cross-shaped buildings: effect of building shape, separation and orientation. Build. Environ. 101, 45–63. https://doi.org/10.1016/j.buildenv.2016.02.015.